JOURNAL OF VIROLOGY, May 2007, p. 4520–4532 Vol. 81, No. 9
0022-538X/07/$08.00+0 doi:10.1128/JVI.02205-06

Polybasic KKR Motif in the Cytoplasmic Tail of Nipah Virus Fusion Protein Modulates Membrane Fusion by Inside-Out Signaling▽

Hector C. Aguilar,[1] Kenneth A. Matreyek,[1] Daniel Y. Choi,[1] Claire Marie Filone,[4] Sophia Young,[1] and Benhur Lee[1,2,3]*

Department of Microbiology, Immunology, and Molecular Genetics,[1] Department of Pathology and Laboratory Medicine,[2] and AIDS Institute,[3] David Geffen School of Medicine at UCLA, Los Angeles, California 90095, and Department of Microbiology, University of Pennsylvania, Philadelphia, Pennsylvania 19104[4]

Received 6 October 2006/Accepted 31 January 2007

The cytoplasmic tails of the envelope proteins from multiple viruses are known to contain determinants that affect their fusogenic capacities. Here we report that specific residues in the cytoplasmic tail of the Nipah virus fusion protein (NiV-F) modulate its fusogenic activity. Truncation of the cytoplasmic tail of NiV-F greatly inhibited cell-cell fusion. Deletion and alanine scan analysis identified a tribasic KKR motif in the membrane-adjacent region as important for modulating cell-cell fusion. The K1A mutation increased fusion 5.5-fold, while the K2A and R3A mutations decreased fusion 3- to 5-fold. These results were corroborated in a reverse-pseudotyped viral entry assay, where receptor-pseudotyped reporter virus was used to infect cells expressing wild-type or mutant NiV envelope glycoproteins. Differential monoclonal antibody binding data indicated that hyper- or hypofusogenic mutations in the KKR motif affected the ectodomain conformation of NiV-F, which in turn resulted in faster or slower six-helix bundle formation, respectively. However, we also present evidence that the hypofusogenic phenotypes of the K2A and R3A mutants were effected via distinct mechanisms. Interestingly, the K2A mutant was also markedly excluded from lipid rafts, where ~20% of wild-type F and the other mutants can be found. Finally, we found a strong negative correlation between the relative fusogenic capacities of these cytoplasmic-tail mutants and the avidities of NiV-F and NiV-G interactions ($P = 0.007$, $r^2 = 0.82$). In toto, our data suggest that inside-out signaling by specific residues in the cytoplasmic tail of NiV-F can modulate its fusogenicity by multiple distinct mechanisms.

Nipah virus (NiV) and *Hendra virus* (HeV) are deadly emerging zoonotic viruses belonging to the new *Henipavirus* genus within the family *Paramyxoviridae* (66). NiV infections result in respiratory and neurological symptoms, often leading to fatal encephalitis, the primary reason for death in humans (32, 64). Microvascular endothelial cell syncytium formation is a hallmark of NiV infection, associated with endothelial cell death, vascular inflammation, and necrosis (70). The mortality rate of NiV-infected humans ranges from ~40% in the original outbreaks in Malaysia and Singapore in 1999 to 2000 to ~70% in Bangladesh in 2005 (5, 6). The natural reservoir for NiV has been determined to be fruit bats of the genus *Pteropus* (46), and pigs served as the intermediate amplifying host in the original Malaysian-Singaporean outbreaks. Ominously, even though human-to-human transmission was not documented in the original outbreaks, direct bat-to-human and human-to-human transmissions have been reported in the later outbreaks in Bangladesh (5, 6). NiV is classified as a BSL4 pathogen and has also been designated as a select agent because of its bio- or agroterrorism potential. These characteristics of NiV underscore the need for research and treatment development against this perilous pathogen and the need for understanding of the necessary components and mechanisms of virus-cell and cell-cell fusions in order to inhibit viral infection and spread.

* Corresponding author. Mailing address: Department of MIMG, 3825 MSB, 609 Charles E. Young Drive East, UCLA, Los Angeles, CA 90095. Phone: (310) 206-8792. Fax: (310) 267-2580. E-mail: bleebhL@ucla.edu.

▽ Published ahead of print on 14 February 2007.

For paramyxoviruses, two separate membrane proteins are involved in the fusion process, the attachment protein (H, HN, or G), which binds to the receptor molecule in the target cell membrane, and the fusion protein (F) that actually carries out membrane fusion. For most paramyxoviruses, both F and its homotypic attachment protein are necessary for membrane fusion, except for rare cases like the hyperfusogenic simian virus 5 (SV5) W3A isolate (27, 48). Activation of F is believed to occur through the following three steps: (i) binding of the attachment protein to the receptor, (ii) interaction of the attachment and F proteins (or changes thereof), and (iii) conformational changes in F that mediate membrane fusion. The fusion (F) and attachment (G) envelope glycoproteins in NiV or HeV are both necessary for cell-cell fusion, syncytium formation, and viral entry. G is responsible for binding to its cognate receptor, ephrinB2 (9, 44), and at least for NiV, ephrinB3 can also be used as an alternative receptor (45). The high expression of ephrinB2 on neurons and endothelial cells and the patterns of expression of ephrinB3 in the central nervous system largely account for the cell tropism of NiV and HeV (9, 44, 45). However, much less is known about the components necessary for the subsequent steps in the activation of NiV fusion (NiV-F) or HeV-F protein.

Paramyxovirus F proteins belong to the class I fusion proteins that share several structural and functional characteristics. The structures of the retroviral Moloney murine leukemia virus (MoMuLV) p15E, lentiviral human immunodeficiency virus type 1 (HIV-1) gp41, Ebola virus GP2, paramyxovirus SV5 F, and influenza virus hemagglutinin (HA) fusion proteins have all been shown to have similar trimeric coiled-coil core

structures, suggesting similar membrane fusion mechanisms (8, 14, 20, 72). Class I fusion proteins of enveloped viruses are synthesized as precursors that must be cleaved and hence activated into a metastable conformation that is ready for enabling virus-cell membrane fusion. Typically, cleavage generates a new N terminus that contains a hydrophobic fusion peptide motif. Upon activation of the fusion protein through receptor binding and/or endosomal low pH, the fusion peptide gets inserted into the host cell target membrane. Class I fusion proteins also contain two heptad repeat regions (HR1 and HR2); the C-terminal HR2 region is generally thought to be preformed, but the N-terminal HR1 region is formed only upon fusion peptide insertion (14, 35, 72, 73). Class I fusion proteins function as trimers, and the HR1 and HR2 regions have a strong propensity to fold into coiled-coil domains during six-helix bundle (6HB) formation. The free energy released from fusion protein refolding from the metastable prefusion state to the stable postfusion 6HB state likely drives the virus-host cell membranes together, overcoming the electrostatic repulsion intrinsic to the negatively charged phospholipids' head groups of the two membranes (38, 55).

For NiV and HeV, the fusion protein is cleaved within the endosomal compartment from the precursor F_0 to the F_1 and F_2 subunits (18, 39). Such cleavage is likely required for activation of the F protein into the metastable state. For NiV, after activation into the metastable state, not much is known about the subsequent steps in the triggering of the fusion protein that leads to eventual membrane fusion. We and others have recently reported that N-glycans in both the NiV-F and HeV-F proteins have some effects on protein expression and membrane fusion (3, 15, 40). In addition, we identified N-glycans in NiV-F that both reduce fusion and viral entry and protect the virus against neutralizing antibodies (Abs) (3). These results show some uniqueness of the *Henipavirus* genus fusion proteins. However, little is known about other domains in NiV-F or HeV-F that may have an important role in membrane fusion. Triggering of fusion is usually envisioned to involve primarily the ectodomain of the fusion protein. However, accumulating evidence from retroviral (13, 25, 50, 54), lentiviral (41, 42), and other paramyxoviral (65, 67) envelope (Env) proteins suggests that the Env cytoplasmic tail (CT) is involved in regulating the fusion process.

Multiple reports indicate that fusion mediated by the ectodomain of the retrovirus MoMuLV (2), the lentiviruses simian immunodeficiency virus (SIV) (61) and HIV-1 (71), and the paramyxovirus SV5 (67) fusion proteins can be modulated by inside-out signaling from the CT. Truncation of the long CT of lentiviral Env proteins occurs under certain culture conditions, and increased fusogenicity has been reported for truncated versions of SIV, HIV-1, and HIV-2 Env (16, 31, 41, 60, 61, 76). For the paramyxovirus SV5 F protein, isolates with a short (20-residue) CT (W3A and WR) cause extensive cell-cell fusion, whereas isolates with an extended CT (T1 and SER) cause little or no cell-cell fusion, and truncation of the CT restores fusion to levels seen in W3A and WR isolates (28, 65). For MoMuLV, SIV, and SV5, the hyperfusogenicity caused by truncation of the CT is linked to overall conformational changes in the ectodomain of the protein (2, 61, 67). In MoMuLV and the Mason-Pfizer monkey virus, the CT is even protease cleaved during viral maturation to "prime" the fusion protein for fusogenicity (2, 13). Here we investigated the potential role(s) of the CT of the NiV fusion protein in cell surface expression (CSE), processing, membrane fusion, and viral entry and defined specific residues in a polybasic motif in the CT that can affect the conformation of the ectodomain, fusogenicity, and interaction of the fusion protein with the attachment glycoprotein.

MATERIALS AND METHODS

Expression plasmids and codon optimization. The codon-optimized NiV-G and NiV-F genes were tagged at their C termini with HA and AU1 tags, respectively, as previously described (33). The NiV-HR2-Fc construct was made by fusing the heptad repeat region 2 sequence of NiV-F (amino acids 447 to 488) with the human immunoglobulin G1 Fc constant region as previously described (3, 44). The deletion mutants −T, −T1, −T2, −T3, −T4, −T12, and −T234 and point mutants K1A, K2A, R3A, N4A, and T5A were made by deleting or mutating the codon-optimized wild-type (WT) NiV-F plasmid with appropriately designed primers and the QuikChange site-directed mutagenesis kit (Stratagene, Cedar Creek, TX). All mutations and deletions were confirmed by sequencing the entire open reading frame.

Cell culture. Vero cells were cultured in minimal essential medium alpha with 10% fetal bovine serum (FBS). PK13 and 293T cells were cultured in Dulbecco's modified Eagle's medium with 10% FBS. We obtained 293T and Vero cells from the American Type Culture Collection, and PK13 (porcine fibroblasts) cells were a kind gift from Irvin Chen at the University of California Los Angeles.

Quantitation of cell-cell fusion. Codon-optimized NiV-G and codon-optimized WT or mutant NiV-F expression plasmids (1:1 ratio, 1 μg total) (3, 33) were transfected with 1.5 μg pcDNA3.1 plasmid as filler DNA into 293T or Vero cells growing in 12-well plates at 80% confluence, as indicated. At 12 to 18 h posttransfection, cells were stained with 4′,6′-diamidino-2-phenylindole (DAPI) and syncytium formation was quantified by counting the nuclei in syncytia per ×100 field (at least 10 fields were counted per condition). Syncytia were defined as four or more nuclei visualized within a common cell membrane, as indicated previously (3).

Quantification of NiV-F and NiV-G CSE levels by flow cytometry. Production of antisera from genetically immunized rabbits (with NiV-M and -F or -G expression plasmids) was previously described (44). Sera containing anti-F or anti-G specific activities were used for flow cytometry on NiV-F- or -G-transfected cells at a 1:1,000 dilution. Bound Ab was detected with phycoerythrin-conjugated goat anti-rabbit Abs (Caltag, Burlingame, CA). Antisera were also raised in rabbits immunized with peptides corresponding to amino acids 39 to 57 and 331 to 348 of NiV-F_2 and NiV-G, respectively, as previously described (3, 33). These regions were previously shown to be immunogenic (10). For quantitation of binding of the monoclonal Abs (MAbs), flow cytometry was performed with MAb concentrations of 0.03 to 3 μg/ml. For calculating the binding ratios of any given pair of Abs, data obtained from equal concentrations of the respective Abs were used.

Reverse pseudotype viral entry assay. The ephrinB2 NiV receptor protein was pseudotyped onto a reporter virus, vesicular stomatitis virus (VSV), by transfecting an ephrinB2 expression plasmid into 293T cells and subsequently infecting these cells with recombinant VSV expressing the *Renilla* Luc reporter gene (VSV-ΔG-rLuc), similarly to the procedure described previously for preparation of NiV-F- and -G-pseudotyped VSVrLuc virions (3, 44, 45). ephrinB2 reverse-pseudotyped virions were purified over a 20% sucrose cushion as for NiV-F- and -G-pseudotyped viruses. 293T cells plated in 96-well plates were transfected with NiV-G and WT or mutant NiV-F and, 10 to 12 h later, infected with reverse-pseudotyped virions in phosphate-buffered saline–1% FBS for 2 h at 37°C over a 5-log viral dilution range (10^{-2} to 10^{-6}). After 2 h, cells were washed and 293T cell growth medium was added. At 24 h postinfection, cells were lysed and luciferase activity was measured as relative light units (RLU) with a *Renilla* luciferase detection system (Promega, Madison, WI) and a Veritas microplate luminometer (Turner Biosystems, Sunnyvale, CA). Quantitation of viral genome copies for the ephrinB2 VSV-pseudotyped viral prep was performed exactly as previously described (3). For quantitation of neutralization of viral entry, the reverse-pseudotyped viral entry assay was performed as described above, except in the presence of the indicated amounts of the specified Abs. For the mixed heterotrimer experiments with the K1A and K2A or R3A mutant proteins, the indicated DNA ratios of the expression plasmids for the indicated proteins were transfected into 293T cells 18 h before infection with the reverse-pseudotyped virions.

Western blot analysis of surface NiV-F and NiV-G proteins. Codon-optimized NiV-F and/or NiV-G expression plasmids (1:1 ratios when in combination) were transfected into 293T cells plated in six-well plates (total of 2 μg F and/or G plasmids with 3 μg PCDNA3.1 plasmid as filler DNA/well), as indicated. Cells were either cell surface biotinylated or not (EZ link Sulfo-NHS-LC-Biotin; Pierce, Rockford, IL), as specified, and biotinylated proteins were precipitated with streptavidin-agarose beads (Pierce, Rockford, IL). Twenty percent of the biotinylated cell lysate was subjected to sodium dodecyl sulfate-polyacrylamide gel electrophoresis and subsequently detected by Western blotting with anti-tag (HA or AU1), anti-F_2, or anti-G peptide Abs, as indicated. Primary and secondary Abs were used at 1:1,000 and 1:20,000 dilutions, respectively, followed by ECL Plus detection (Amersham Biosciences, Piscataway, NJ). For quantification of relative processing levels for the various NiV-F proteins, the ratio of the densitometric units of the F_1 subunit over those of the sum of the precursor F_0 and the F_1 subunits was calculated.

Lipid raft association of NiV-F proteins. 293T cells transfected with WT or mutant NiV-F proteins (as described above) were washed with phosphate-buffered saline and resuspended in TNE buffer (25 mM Tris [pH 7.5], 150 mM NaCl, 5 mM EDTA) containing a protease inhibitor cocktail (Roche, Indianapolis, IN). Cells were Dounce homogenized, and their nuclei were isolated and discarded. Postnuclear supernatants were treated with 1% Triton X-100 for 30 min at 4°C. Cell lysates were then brought up to a 40% OptiPrep (Sigma-Aldrich, St. Louis MO) concentration in 1.2 ml, placed at the bottom of an ultracentrifuge tube, and layered sequentially with 30% (3 ml) and 5% (0.8 ml) OptiPrep layers (in TNE buffer plus protease inhibitors). These discontinuous gradients were centrifuged at 45,000 rpm for 16 h at 4°C in an SW50.1 rotor. After centrifugation, 12 equal fractions were manually collected from the top, protein from 200 μl of each fraction was precipitated by a methanol-chloroform extraction method (69), and each fraction was analyzed by Western blotting. The overall lipid raft domain isolation procedure was similar to that used by Fleming et al. (22).

Production of NiV-HR2-Fc immunoadhesin and fusion inhibition. The NiV-HR2-Fc expression plasmid was transfected into 293T cells, and at 24 h posttransfection, supernatants were collected and concentrated with a Centriplus YM-10 filter (Millipore, Bedford, MA). Protein concentrations were measured by an Fc-specific enzyme-linked immunosorbent assay as previously described (44). For NiV fusion inhibition, the indicated amounts of NiV-HR2-Fc were added to 293T cells transfected with NiV-G and WT or N-glycan mutant NiV-F expression plasmids. Fusion was quantified after overnight incubation as described above.

Fusion kinetics of WT or mutant NiV-F proteins. The fusion kinetics of WT and mutant NiV-F proteins were determined in a β-lactamase reporter cell-cell fusion assay as previously described (3, 34, 53). For better sensitivity, the β-lactamase gene was also codon optimized for mammalian cell expression (Geneart, Inc., Toronto, Ontario, Canada). Fusion-nonpermissive PK13 effector cells were cotransfected with β-lactamase, NiV-G, and WT or mutant NiV-F expression constructs with Lipofectamine 2000. These were then added to 293T target cells labeled with CCF2-AM dye. Effector and target cells were mixed and incubated at 37°C, and cell-cell fusion was detected by analyzing the shift from green to blue fluorescence, indicating β-lactamase cleavage of CCF2. Fluorescence was quantified every 3 min with a CytoFluor Series 4000 Fluorescence multiwell plate reader (PerSeptive Biosystems, Framingham, MA). The results are expressed as the ratio of blue to green fluorescence obtained with NiV-G- and NiV-F-transfected effectors minus the background blue and green fluorescence obtained with empty-vector-transfected cells.

NiV-F–NiV-G coimmunoprecipitation. 293T cells in 10-cm plates were transfected with 20 μg of the indicated NiV-F-G plasmids at a 1:1 ratio with Lipofectamine 2000. At 24 h posttransfection, cells were lysed and cell lysates were subjected to immunoprecipitation as previously described (3, 33), with a 1:100 dilution of anti-NiV-G peptide serum. Coimmunoprecipitated (co-IP) proteins were analyzed by Western blotting with the appropriate anti-tag Ab as described above and then quantified by densitometry with a VersaDoc Imaging System (Bio-Rad, Hercules, CA).

RESULTS

The membrane-proximal region in the CT of the NiV fusion protein plays a role in membrane fusion. The CT of NiV-F can be conveniently divided into four distinct regions, i.e., a membrane-proximal polybasic region (T1), a functional tyrosine-based endocytic motif (YSRL) (18, 39), a highly charged region (T3), and a C-terminal region that is rich in polar residues (T4). To investigate the potential roles that these cytoplasmic regions may play in membrane fusion, protein expression, processing, and transport, we made a series of deletion mutants that lack various regions of the CT, as illustrated in Fig. 1A. The first amino acid of the CT is a glutamic acid and is likely required to demarcate the membrane-spanning domain. Thus, we kept this amino acid in every deletion mutant in order to maximize the likelihood of correct protein folding and expression. We then analyzed the relative levels of CSE and processing of such deletion mutants and compared them to those of WT NiV-F.

Briefly, 293T cells transfected with expression plasmids for WT NiV-F or the indicated mutant proteins were cell surface biotinylated and lysed and cell surface proteins were precipitated with streptavidin beads and then NiV-F detected by Western blotting with the specified Abs (Fig. 1B). Alternatively, we performed flow cytometric analysis on parallel samples of 293T cells expressing WT NiV-F or the deletion mutants with polyclonal anti-NiV-F antiserum 834, which was previously described (3, 33, 45) (Fig. 1D). Both biotinylation and flow cytometric CSE analyses indicated that the deletion mutants were expressed to at least 50% of the WT level and some were even expressed at levels higher than that of the WT. The cell surface biotinylation experiments also showed that the deletion mutants were cleaved and processed more or less at WT levels, with the exception of the deletion mutant missing the entire CT (Fig. 1B, bottom). Interestingly, although this deletion mutant (−T) did not include removal of the C-terminal AU1 tag, the anti-AU1 MAb was not able to detect this protein by Western blotting, perhaps because of the close proximity of the AU1 tag to the detergent-lipid micelles (Fig. 1B, top left part). However, the −T mutant was clearly expressed, as shown by blotting with an anti-F_2 peptide antiserum previously described (3, 33) (Fig. 1B, right part), as well as by flow cytometry (Fig. 1D). Notably, the −T mutant was also not processed efficiently despite being expressed on the cell surface (Fig. 1B, right part).

Cleavage of NiV-F requires active endocytosis and processing by endosomal cathepsin L, which is in part mediated by the YXXΦ endocytic motif in the T2 region (18, 39). Since the AU1 tag contains a putative YXXΦ endocytic motif, we sought to determine if our AU1 tag had any inadvertent effects on the expression or processing of NiV-F. Figure 1C shows that there were no differences in cleavage or processing efficiency between tagged and untagged WT NiV-F (F and F_{NA}, respectively). Interestingly, the untagged version of the T2 mutant ($-T2_{NA}$), which lacks the endogenous YXXΦ motif, also showed no differences from untagged WT NiV-F (F_{NA}), similar to what has been found with the tagged versions (compare Fig. 1B and C).

Next, we asked whether the CT deletion mutations affected the fusogenicity of the NiV-F fusion protein. To normalize for the differences in CSE, we compared the fusion-to-CSE ratios induced by WT NiV-F and the indicated deletion mutants (Fig. 1D). We performed our syncytium-forming assays by transfecting in 0.3 μg of NiV-F and -G per 12-well plate, which was previously determined to result in CSE and fusion with the WT NiV-F protein in the linear range of measurement (3). CSE was measured by flow cytometry as described above, and fusion was determined by counting nuclei inside syncytia (more than

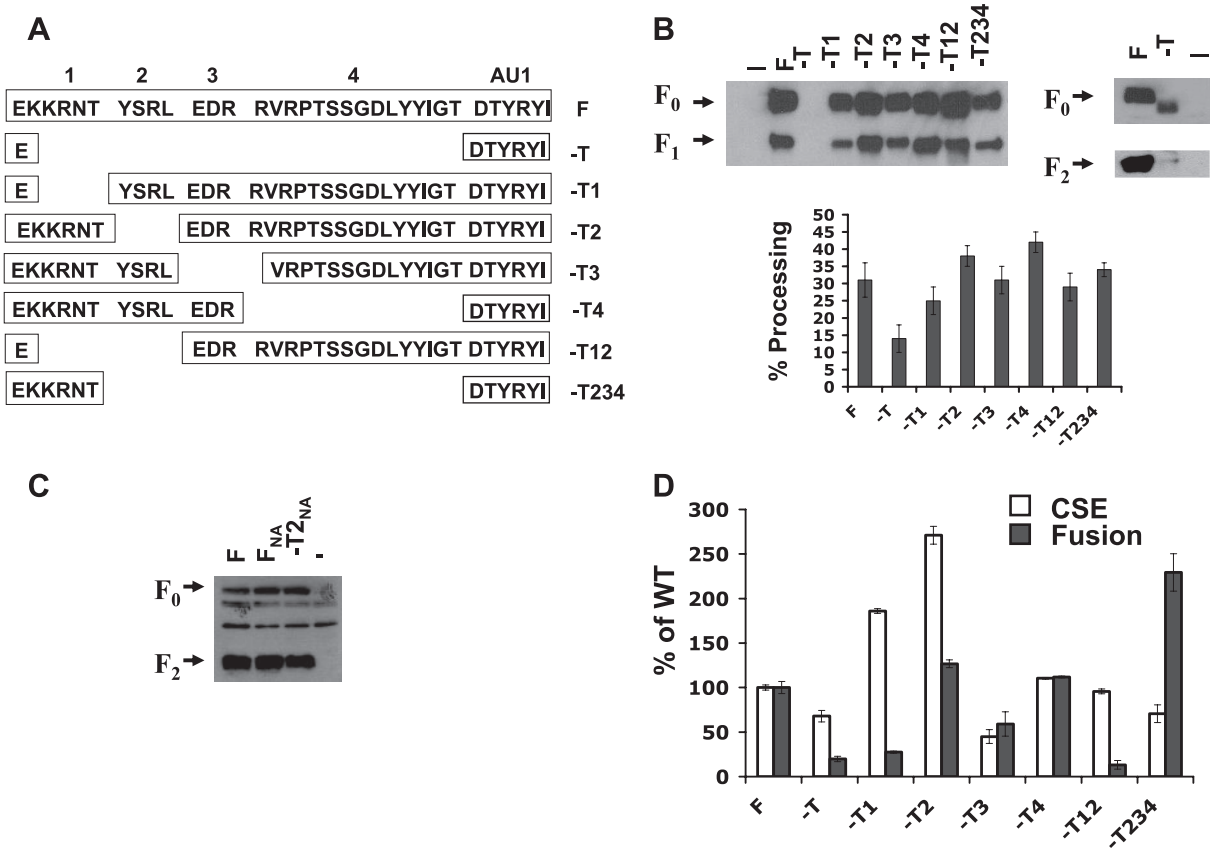

FIG. 1. Analysis of NiV-F CT deletion mutants. (A) Schematic of the NiV-F CT deletion mutants. NiV-F CT was divided into four regions (numbered 1, 2, 3, and 4) as described in the text, and the names of the deletion mutants examined are indicated. (B) Western blot analysis of immunoprecipitated surface WT and mutant NiV-F proteins. Briefly, biotinylated cells were lysed, cell surface biotinylated proteins were precipitated with streptavidin agarose beads, and NiV-F was detected in the biotinylated precipitates by Western blotting with either a monoclonal anti-AU1 tag Ab (left part) or a rabbit anti NiV-F_2 antipeptide Ab (3) (right part). Percent processing was calculated as the densitometric units of the F_1 subunit over those of the sum of the precursor F_0 and the F_1 subunits (bottom part) ($n = 3$). (C) The AU1 tag does not affect cleavage and processing of F. Identical cell surface biotinylation experiments were performed with tagged (F) and untagged versions of WT F (F_{NA}) and the −T2 mutant ($-T2_{NA}$). A rabbit anti NiV-F_2 antipeptide Ab (3) was used to detect NiV-F. (D) Relative levels of CSE and fusion obtained for WT NiV-F and the indicated CT deletion mutants. Fusion was determined by counting nuclei in syncytia per field. At least 10 fields were counted per condition. CSE was determined by flow cytometry with polyclonal anti-NiV-F specific antiserum as described previously (3). Both CSE and fusion levels were separately normalized to levels of WT NiV-F protein, set at 100%. Data shown are averages ± standard errors from three independent experiments.

four nuclei per cell) per microscopic field, respectively. Figure 1D shows the relative CSE and fusogenicity of WT NiV-F and the indicated mutants, and Table 1 (top) shows their corresponding fusion/CSE ratios. Interestingly, all mutants that lacked the membrane-proximal T1 region (−T1 and −T12) were hypofusogenic and had fusion/CSE ratios of less than 0.5 (by definition, that of WT NiV-F is 1.0), while all mutants that retained the T1 region (−T3, −T4, and −T234) had fusion/CSE ratios equal to or higher than that of WT NiV-F, with the exception of the −T2 mutant, which had a fusion/CSE ratio of 0.5. Since the fusion defect in the tailless mutant (−T) was likely due at least partially to its processing defect, it was not included in Table 1 for comparison. These results indicate that the CT, in particular, the membrane-proximal T1 region of the CT, plays an important role in membrane fusion and syncytium formation.

Polybasic KKR motif in the membrane-proximal region of the NiV-F CT modulates NiV-F-induced membrane fusion. To

TABLE 1. Fusion/CSE ratios

Env fusion protein	Fusion/CSE ratio[a]
F	1.0
−T1	0.1
−T2	0.5
−T3	1.3
−T4	1.0
−T12	0.1
−T234	3.2
K1A	5.5
K2A	0.2
R3A	0.3
N4A	0.9
T5A	0.9

[a] The ratio of the normalized fusion and CSE values for each mutant was calculated from the data in Fig. 1D and 2C. By definition, the fusion/CSE ratio for WT NiV-F would be 1.0 (100%/100%). Ratios of >1 indicate increased fusogenicity, while mutants with decreased fusogenicity would have ratios of <1.

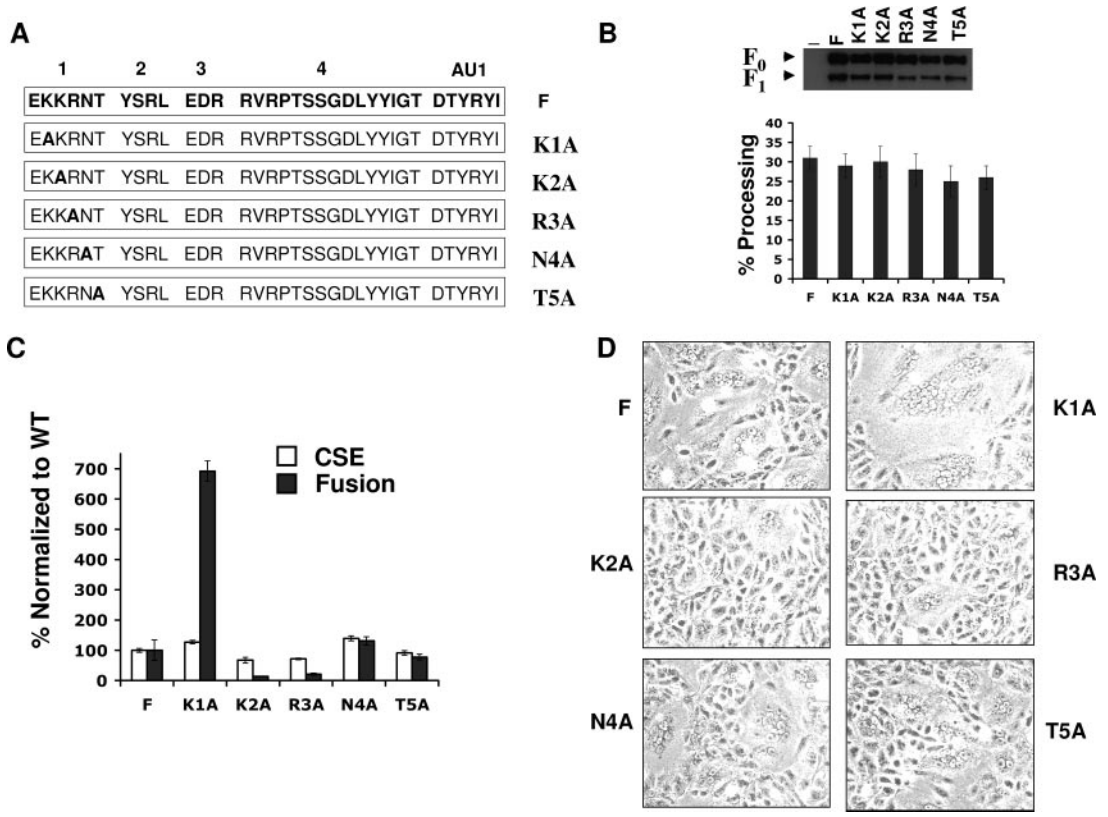

FIG. 2. Analysis of membrane-proximal point mutations in the CTs of NiV-F. (A) Schematic of the NiV-F CT point mutants, showing the sequence of the whole CT, and the positions of the five alanine substitutions in the membrane-proximal region, designated K1A, K2A, R3A, N4A, and T5A. (B) Western blot analysis of immunoprecipitated cell surface biotinylated WT and mutant NiV-F proteins. Surface proteins were analyzed exactly as described in Fig. 1B. Percent processing was also analyzed as described in the legend to Fig. 1B, and the densitometric results are shown graphically. (C) Relative levels of CSE and fusion obtained for WT NiV-F or CT point mutant proteins in 293T cells. Fusion and CSE were determined exactly as for Fig. 1C. Data shown are averages ± standard errors from three independent experiments. (D) Pictures of syncytium formation by the WT NiV-F or the various NiV-F point mutants and WT NiV-G in Vero cells. Representative ×100 fields are shown.

finely map the particular residues within the T1 region that can modulate NiV-F-mediated fusion, we individually mutated each amino acid of the T1 sequence (KKRNT) to an alanine, as depicted in Fig. 2A. 293T cells transfected with an expression plasmid encoding each of the alanine scan mutants were cell surface biotinylated, lysed, precipitated with streptavidin, and subjected to Western blotting to detect NiV-F as described above. All of the alanine scan mutants had levels of CSE and processing similar to those of WT NiV-F (Fig. 2B). Similar levels of CSE of WT and mutant NiV-F proteins were also observed by flow cytometric analyses (Fig. 2C). Next, we determined the fusogenicity of these mutants by quantifying syncytium formation. Representative pictures of syncytia formed by each mutant are shown in Fig. 2D, and the fusion/CSE ratios for WT NiV-F and the indicated mutant were determined (Table 1, bottom). Interestingly, despite WT levels of CSE, mutation of the K1 residue resulted in hyperfusogenicity (fusion/CSE ratio of 5.5) while mutation of the K2 or R3 residue resulted in hypofusogenicity (fusion/CSE ratios of 0.2 and 0.3, respectively) (Table 1, bottom). Mutation of the N4 or T5 residue did not result in any significant change in CSE or fusion (ratio of 0.9) relative to the WT NiV-F protein (Fig. 2C and D and Table 1, bottom). Similar but less dramatic effects on fusogenicity were observed in Vero cells. In summary, these results indicate that the membrane-proximal polybasic KKR sequence in the CT of NiV-F protein can up- or downmodulate its fusogenicity.

Fusion of membrane-proximal NiV-F mutants correlates with entry of ephrinB2-reverse-pseudotyped virus-like particles. Next, we sought to determine if the differences in cell-cell fusion exhibited by the NiV-F CT mutant proteins corresponded to viral entry differences. However, some of these CT mutants were very inefficiently incorporated into our pseudotyped VSV-*Renilla* luciferase (VSVrLuc) reporter viruses, a previously established method for examining NiV envelope-mediated entry (3). To circumvent the problem of variable envelope protein incorporation into VSVrLuc, we developed a novel reverse-pseudotype VSVrLuc entry assay, for which we reverse pseudotyped VSVrLuc with the NiV receptor ephrinB2 (B2-VSVrLuc). We then used these B2-VSVrLuc virions to infect 293T cells previously transfected with equal amounts of mutant or WT NiV-F along with WT NiV-G in a 96-well plate format. Infection of cells expressing HIV Env glycoproteins with viral particles reverse pseudotyped with CD4 and the corresponding coreceptor has been previously reported (36, 56). Figure 3A shows that B2-VSVrLuc viral entry only occurs when cells express both the NiV-F and NiV-G glycoproteins (Fig. 3A). In addition, reverse-

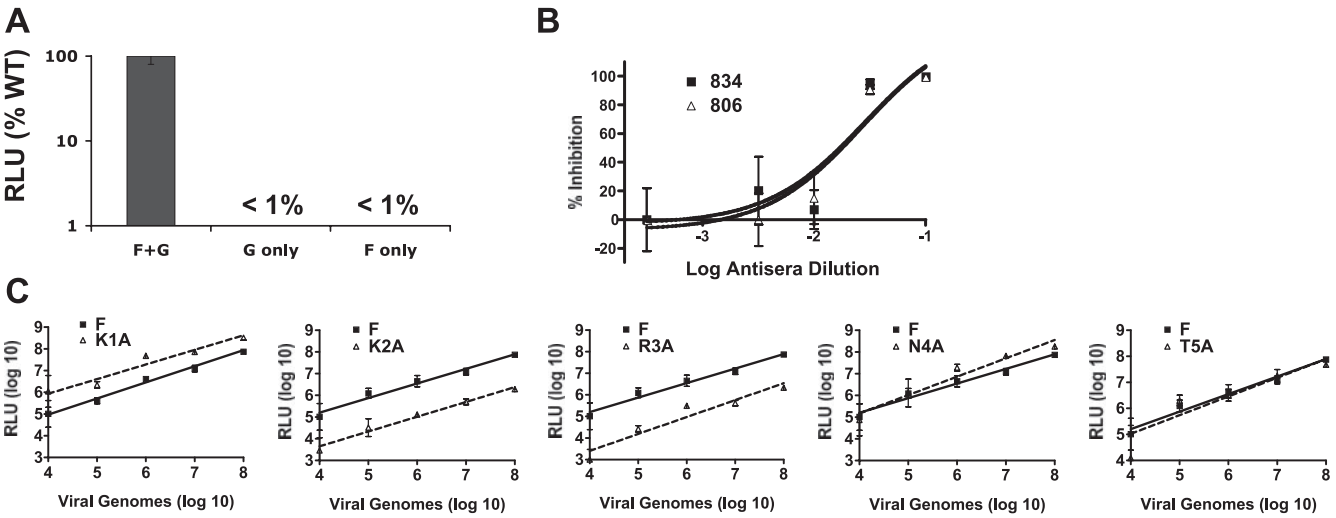

FIG. 3. Reverse-pseudotyped viral entry assay for membrane-proximal CT point mutants. (A) An ephrinB2-pseudotyped VSV-*Renilla* luciferase reporter virus (B2-VSV-rLuc) was used to infect 293T cells previously transfected with expression plasmids for NiV-F–NiV-G, NiV-G alone, or NiV-F alone. Numbers of RLU are shown on a logarithmic scale. (B) Reverse-pseudotyped viral entry into NiV-F- or NiV-G-transfected 293T cells was inhibited by anti-NiV-F and anti-NiV-G specific antisera 834 and 806, respectively. Data are presented as percent inhibition, where 0% represents infection in the absence of any antiserum. The data were normalized as follows. The number of RLU obtained at each serum dilution was calculated as a percentage of the average number of RLU obtained in the absence of any antiserum. Percent inhibition was then calculated as 100% minus the percent infection at each serum dilution. The percent inhibition values were regressed and graphed with GraphPad PRISM. An average of two experiments is shown, with four independent wells per datum point (serum dilution) ± the standard deviation. (C) Relative entry levels of B2-VSV-rLuc virus into 293T cells expressing the WT NiV-G protein and the WT or mutant NiV-F protein. RLU were quantified 24 h postinfection and graphed against the number of viral genomes per milliliter. A single preparation of B2-VSV-rLuc was used for all of the experiments shown. The number of genome copies in the viral preparation was analyzed by reverse transcription-PCR as described in Materials and Methods. The data shown are averages from three independent experiments ± the standard deviations.

pseudotyped viral entry was specifically blocked by previously characterized anti-NiV-F or anti-NiV-G antiserum (3, 33, 44) (Fig. 3B).

We then determined the entry of these B2-VSVrLuc virions into cells expressing WT NiV-G and WT NiV-F or the indicated NiV-F CT point mutants. Entry into K1A-expressing cells was about 8- to 10-fold higher than that of WT NiV-F over several logs of viral input. Conversely, entry into K2A- and R3A-expressing cells was 8- to 30-fold lower than that of WT NiV-F over the same range of viral inputs. Entry levels obtained for the cells expressing the N4A or T5A mutant protein were similar to those expressing WT NiV-F. Thus, our reverse-pseudotype B2-VSVrLuc entry assay results are consistent with our cell-cell fusion results and further demonstrate that the membrane-proximal polybasic KKR motif in the NiV-F CT can modulate virus-cell membrane fusion.

Differential binding and neutralization of hyper- and hypofusogenic NiV-F mutants by distinct novel anti-NiV-F rabbit MAbs. We then asked how specific residues in the KKR region might be modulating fusion. Inside-out signaling from the CT has been reported for other class I enveloped viruses (2, 61), including at least one paramyxovirus (67). We first asked whether any of the KKR alanine mutations affected the overall ectodomain conformation of the NiV-F protein.

We had previously produced conformational polyclonal and monoclonal rabbit Abs by genetically immunizing rabbits with codon-optimized NiV-F and NiV-G and NiV-M expression plasmids (4). We screened a panel of our rabbit MAbs and found two (MAbs 92 and 66) whose epitopes were conformational and distinct. They were conformational because they detected the NiV-F protein in its native state by flow cytometry (Fig. 4A) but not in its denatured form, for example, by Western blot analysis on sodium dodecyl sulfate-polyacrylamide gel electrophoresis (data not shown). They were distinct because Ab 66 bound to NiV-F and HeV-F equivalently while Ab 92 bound to NiV-F approximately10-fold more efficiently than to HeV-F at the same Ab concentrations (Fig. 4A). As a control, polyclonal Ab 834 (3, 33, 44) was used to show that the levels of NiV-F and HeV-F were approximately equally recognized by flow cytometry in the same experiment (Fig. 4A).

Then we measured the relative binding of these Abs to the various WT or mutant NiV-F proteins by flow cytometry. We reasoned that conformational differences in the ectodomain might be revealed by differential binding of these Abs. In order to quantitatively correct for variations in the transfection efficiencies and cell surface protein expression levels of the various mutants from experiment to experiment, we analyzed the binding data obtained by calculating the ratios of the mean fluorescence intensities of pairs of Abs (92-66, 92-834, and 66-834). Figure 4B shows the relative binding ratios of thee Ab combinations for WT NiV-F and the indicated mutants. There was a modest but significant decrease in binding of MAb 92 to the hyperfusogenic K1A mutant, as the 92/834 and 92/66 ratios, but not the 66/834 ratio, were lower than those of the WT NiV-F protein ($P = 0.015$, $P = 0.0005$, and $P = 0.94$, respectively) (Fig. 4B). We also detected an increase in binding of MAb 66 to the hypofusogenic R3A mutant protein, as the 66/834 ratio for this mutant was increased, the 92/66 ratio was decreased, and the 92/834 ratio was unchanged compared to those obtained with the WT NiV-F protein ($P = 0.048$, $P =$

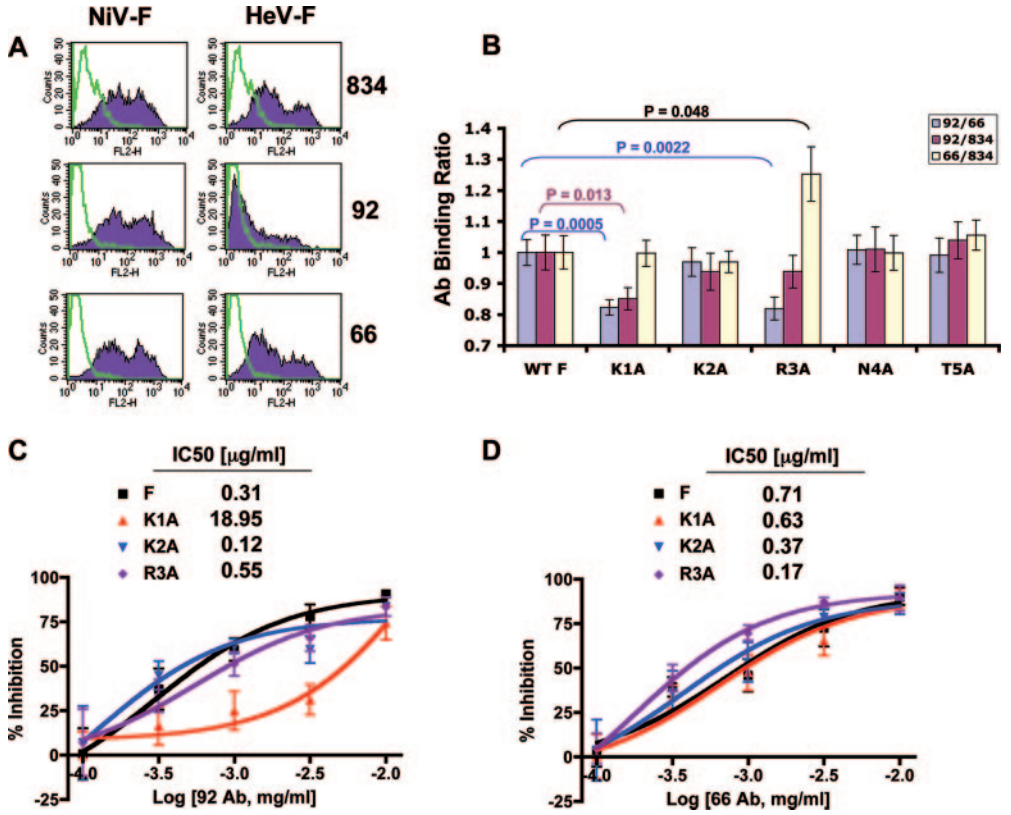

FIG. 4. Specific CT mutants affect the ectodomain conformation as exhibited by differential MAb binding and neutralization. (A) Flow cytometry histograms showing binding of polyclonal anti-NiV-F antiserum 834 or anti-NiV-F MAb 92 or 66 to 293T cells expressing either NiV-F, HeV-F, or neither (pcDNA3 control). Green contours indicate binding of Abs to 293T cells transfected with the pcDNA3.1 backbone only. Overlaid filled purple histograms indicate binding of Abs to NiV-F- or HeV-F-expressing cells, as indicated. (B) MAb binding ratios of pairs of anti-NiV-F Abs. Polyclonal (antiserum 834) or monoclonal (antisera 492 and 66) rabbit Abs were used to stain 293T cells transfected with WT NiV-F or the indicated CT point mutants at a concentration previously determined to be in the linear range of the binding curve. To compare data from repeat experiments and to control for transfection efficiency and differential expression, a set of binding ratios was calculated by dividing the mean fluorescence intensities obtained for the various Abs (92/66, 92/834, and 66/834). The Ab binding ratios for WT NiV-F is necessarily defined as 1. *P* values were calculated with a nonpaired Student *t* test and multiplied by five, which takes into account the Bonferroni correction for the multiple pairwise comparisons (WT versus the five mutants). (C and D) Neutralization of CT mutant proteins by anti-NiV-F Abs. 293T cells expressing the WT NiV-G protein and the WT or mutant NiV-F protein were infected with B2-VSV-rLuc reverse-pseudotyped virus 8 h posttransfection in the presence of increasing amounts of MAb 92 (C) or 66 (D). The amount of viral entry obtained in the absence of anti-NiV-F MAb (artificially represented by the [MAb] = −4.0 datum point) was normalized to 100%, which is equivalent to 0% inhibition. The percent inhibition was then plotted against the logarithm of the Ab concentration. Inhibition curves were regressed, and IC_{50}s were calculated with GraphPad PRISM. The data shown are normalized averages from three separate experiments ± the standard deviations.

0.0022, and $P = 0.84$, respectively) (Fig. 4B). All other point mutant proteins did not display a change in Ab binding relative to that of the WT NiV-F protein (*P* values of >0.5) (Fig. 4B). Similar Ab binding ratios were obtained over an Ab concentration range of 0.03 to 3 μg/ml, and the data shown are for 1 μg/ml.

Next, we measured the neutralization capabilities of MAbs 92 and 66 against the various mutant proteins with our reverse-pseudotyped viral entry assay. In general, our neutralization data were consistent with the above-mentioned binding data. For example, since MAb 92 bound relatively less to mutant K1A, we expected that mutant K1A may also be less sensitive to neutralization by MAb 92, and that was indeed the case. Figure 4C shows that the K1A protein was more than 10-fold less sensitive than WT NiV-F to neutralization by MAb 92 (the 50% inhibitory concentrations [IC_{50}s] for K1A and WT NiV-F were approximately 19 and 0.3 μg/ml, respectively). In addition, since MAb 66 bound more strongly to mutant R3A, we also expected that the R3A mutant might also be more sensitive to neutralization by MAb 66 than the WT NiV-F. Indeed, we observed that the R3A mutant protein was about fourfold more sensitive to neutralization by MAb 66 than was the WT NiV-F protein, as the IC_{50}s for the R3A and WT proteins were approximately 0.17 and 0.71 μg/ml, respectively (Fig. 4D). In toto, our MAb binding and neutralization data show that specific residues in the CT of NiV-F can affect the conformation of its ectodomain.

Association of NiV-F and the hyper- and hypofusogenic mutants with lipid raft domains. Viral envelope glycoproteins are often associated with lipid raft microdomains (22, 26, 43, 47, 62). Such membrane domains are known to have membrane cross-thicknesses greater than those of non-lipid raft cell membrane domains (23, 30) and are enriched in cholesterol and glycosphingolipids. Thus, differential association of WT or mu-

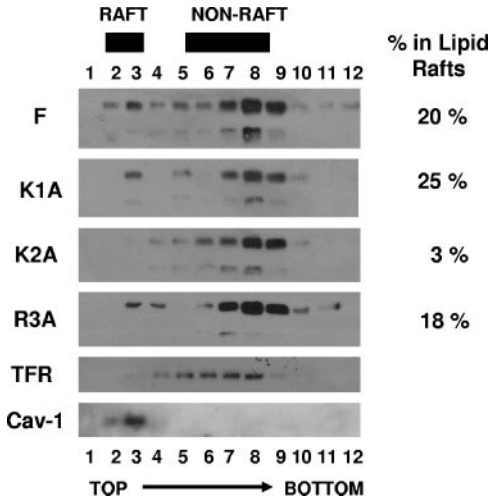

FIG. 5. Association of NiV-F and the hyper- and hypofusogenic mutants with lipid raft domains. Lipid raft fractionations were performed as described in Materials and Methods. Caveolin-1 (Cav-1) and transferrin receptor (TFR) were used as markers for raft (top) and nonraft (bottom) domains, respectively. NiV-F and the indicated mutants were detected by Western blotting with the AU1 Ab. The blots were then stripped and reprobed for Cav-1 and TFR to ensure the integrity of each lipid raft fractionation. Percent NiV-F in lipid rafts was calculated as the percentage of the NiV-F signal observed in the peak Cav-1 fractions (lanes 2 and 3 in most cases) over the sum of signals in the peak Cav-1 and peak TFR fractions (lanes 7 and 8 in most cases) for each sample. This controls for any slight variations between tubes. Representative Cav-1 and TFR blots are shown. The experiment was repeated twice with similar results. Band intensities were quantified by densitometry with a VersaDoc Imaging System (Bio-Rad).

tant NiV-F proteins with lipid raft domains may formally influence the conformation of their ectodomain epitopes, potentially affecting the conformational data in Fig. 4. Therefore, we assessed the relative association of WT and mutant NiV-F proteins with lipid raft domains. First, we observed that a distinct portion (~20%) of the total WT NiV-F protein was associated with lipid raft fractions (Fig. 5), as demonstrated by cofractionation with caveolin-1, a standard marker for lipid raft domains. However, the most of the NiV-F was in nonraft fractions, which were demarcated by the transferrin receptor, a membrane protein known not to be associated with lipid rafts (Fig. 5). With the exception of mutant K2A, all WT and mutant NiV-F proteins were found in both lipid raft and non-lipid raft domains at approximately equal distributions (18 to 25% in lipid raft fractions), indicating that, at least for mutants K1A and R3A, association with lipid rafts did not account for the differences in conformational MAb binding seen in Fig. 4. Interestingly, the hypofusogenic K2A mutant was almost completely absent from the lipid raft fractions, raising the possibility that altered association with lipid raft domains may contribute to its hypofusogenic phenotype and suggesting that mechanistic differences may underlie the hypofusogenic phenotypes of the K2A and R3A mutants.

NiV-F CT fusion mutants are differentially resistant to fusion inhibition by a reagent that prevents 6HB formation and exhibit corresponding rates of fusion kinetics relative to WT NiV-F. Having determined that the specific residues in the CT can affect the ectodomain conformation of NiV-F, we then asked whether the hyper- and hypofusogenic phenotypes exhibited by the NiV-F CT point mutants are mediated by fusion determinants in the ectodomain such as 6HB formation. We have previously shown that a soluble NiV-HR2-Fc protein (HR2 region of NiV-F linked to the Fc constant region of human immunoglobulin G1) inhibits NiV fusion specifically and that the sensitivity of inhibition by this protein inversely correlated with the fusion kinetics of the hyperfusogenic NiV-F N-glycan fusion proteins (3). With the same NiV-HR2-Fc inhibitory reagent, we tested the sensitivity of NiV-F CT mutants or WT NiV-F to fusion inhibition. We observed that the K1A mutant exhibited significantly greater resistance to NiV-HR2-Fc than WT NiV-F for all three concentrations of HR2-Fc tested (Fig. 6A). On the other hand, the K2A mutant exhibited a significantly lower resistance to NiV-HR2-Fc (Fig. 6A), especially when subsaturating amounts of HR2-Fc were

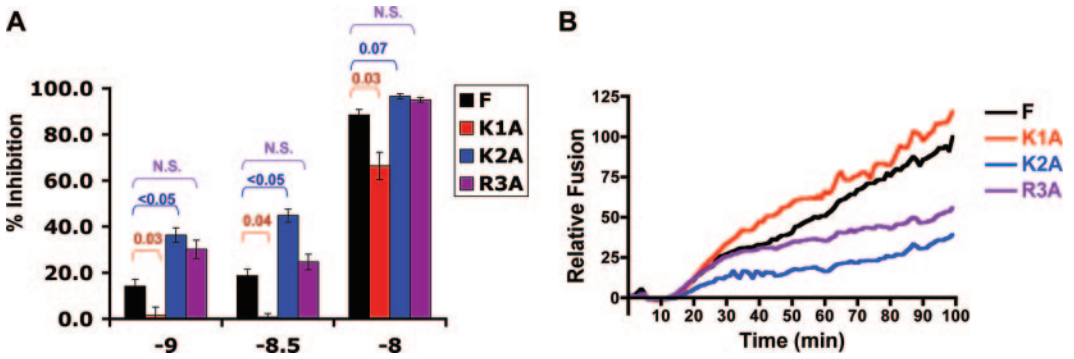

FIG. 6. NiV-F CT fusion mutants are differentially resistant to fusion inhibition by NiV-F HR2-Fc and exhibit corresponding rates of fusion kinetics relative to WT NiV-F. (A) The sensitivity of NiV envelope-mediated fusion to inhibition by NiV-HR2-Fc is shown for WT NiV-F and the indicated CT mutants. For each fusion protein, the amount of fusion in the absence of any inhibitor is set at 0% inhibition. One representative experiment out of two is shown. Error bars indicate standard deviations. *P* values were calculated with the Student *t* test and the Bonferroni correction to account for the multiple pairwise comparisons of significance (F versus K1A, F versus K2A, and F versus R3A). (B) Fusion kinetics of WT or mutant NiV-F protein. NiV-G was expressed with WT NiV-F or the indicated mutants in effector PK13 cells, and the relative rate of fusion was assessed with target 293T cells loaded with CCF2 dye (see Materials and Methods). Relative fusion is the ratio of blue to green fluorescence obtained with NiV-G- and NiV-F-transfected effectors minus the ratio of background blue and green fluorescence obtained with empty-vector (pcDNA3)-transfected cells. Each datum point is an average from three independent experiments.

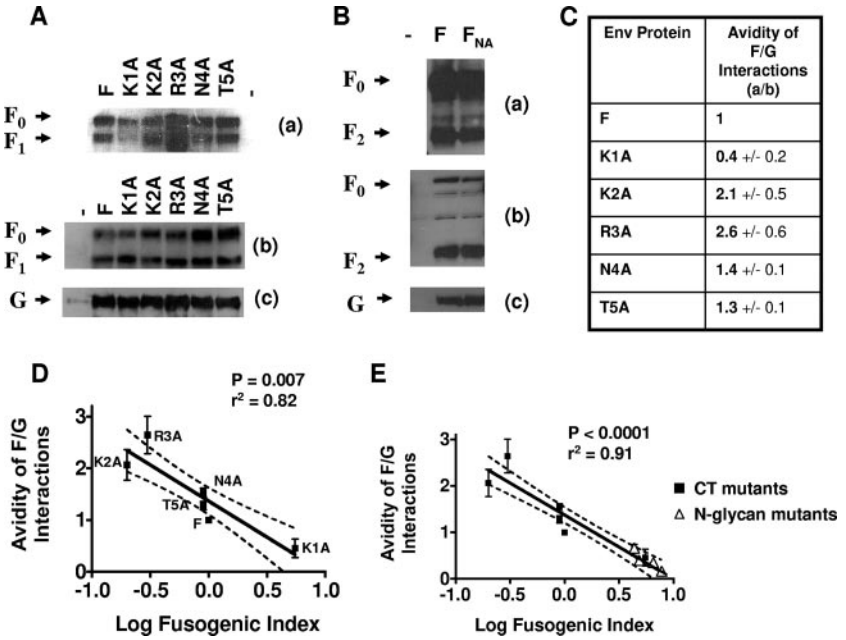

Env Protein	Avidity of F/G Interactions (a/b)
F	1
K1A	0.4 +/- 0.2
K2A	2.1 +/- 0.5
R3A	2.6 +/- 0.6
N4A	1.4 +/- 0.1
T5A	1.3 +/- 0.1

FIG. 7. Fusogenicity of WT NiV-F and the CT mutants inversely correlates with the avidity of F-G interactions. (A) Western blot analysis of co-IP F_0 and F_1 (top part a), immunoprecipitated G (bottom part c), and the relative amounts of F_0 and F_1 present in total cell lysate (middle part b). Cell lysates of 293T cells transfected with WT NiV-G and NiV-F or the indicated CT mutants were immunoprecipitated with rabbit anti-NiV-G specific antisera. The top and middle parts were blotted with mouse anti-AU1 to detect NiV-F, and the bottom part was blotted with mouse anti-HA to detect NiV-G. (B) A coimmunoprecipitation experiment identical to that in panel A was performed with tagged and untagged NiV-F (F and F_{NA}, respectively) but with a rabbit anti-F_2 peptide Ab for detection. Parts a, b, and c are as in panel A. (C) Relative avidities of NiV-F–NiV-G interactions for WT NiV-F and the indicated CT mutants. The amounts of co-IP NiV fusion proteins in panel A were quantified by densitometry as described in the text, with a VersaDoc Imaging System (Bio-Rad). The avidity of F-G interactions is represented by the ratio of the amount of NiV-F protein co-IP with anti-NiV-G antiserum to the relative amount of NiV-F expressed in cell lysates (parts a and b, respectively). The data presented are averages ± standard errors from three experiments. (D) Avidity of the F-G interactions from panel C plotted against the fusion/CSE ratios from Table 1. Pearson correlation analysis was performed with GraphPad PRISM. (E) The avidities of F-G interactions for the multiple N-glycan mutants previously reported by Aguilar et al. (3) were overlaid with the datum points from panel C and plotted together against their respective fusogenic indexes. CT mutants and N-glycan mutants are represented by closed and open symbols, respectively. Pearson correlation analysis was performed with GraphPad PRISM.

used. These results suggested that the rate of 6HB formation contributed to the hyper- and hypofusogenicity of the K1A and K2A mutants, respectively. Interestingly, mutant R3A did not reveal a significant difference in resistance to inhibition by the NiV-HR2-Fc molecule relative to the WT NiV-F protein, suggesting that the hypofusogenic phenotype of the K2A and R3A mutants may be mediated via distinct mechanisms. This is also consistent with our Ab binding data, which suggest that the K2A and R3A mutants differentially affect ectodomain conformation (Fig. 4B).

In order to determine if sensitivity to NiV-HR2-Fc inhibition is actually due to the rate of 6HB formation and, hence, fusion pore formation, we measured fusion kinetics mediated by NiV-F or the indicated CT mutants and WT NiV-G. Real-time fusion kinetics can be measured and quantified with a β-lactamase reporter cell-cell fusion assay that we previously described for analysis of our hyperfusogenic N-glycan NiV-F mutants (3). We found that cells expressing the hyperfusogenic K1A fusion mutant showed faster fusion kinetics and fused to a greater extent than cells expressing WT NiV-F (Fig. 6B). In contrast, the hypofusogenic K2A mutant showed slower fusion kinetics and fused to a lesser extent than cells expressing the WT NiV-F protein (Fig. 6B). Interestingly, although the cells expressing the R3A mutant fused at the same rate as the WT NiV-F protein for the first 40 min, thereafter, their rates of fusion diverged, with the R3A mutant slowing down significantly such that at 100 min, it had fused at less than 50% of the WT NiV-F level (Fig. 6B). The results in Fig. 6A and B strongly suggest a mechanistic difference between the hypofusogenic phenotypes exhibited by the K2A and R3A mutants.

Fusogenicity of NiV-F inversely correlates to the avidity of F-G interactions for the CT mutant proteins. We had previously provided evidence for the attachment protein displacement model for paramyxoviral entry. At least for NiV, the hyperfusogenic N-glycan mutants appear to have weaker interactions between the NiV-F mutants and NiV-G, allowing greater NiV-F–NiV-G dissociation after receptor binding. Thus, fusogenicity inversely correlated to the avidity of F-G interactions for the hyperfusogenic N-glycan NiV-F mutants (3). Here, we asked if the relative avidity of NiV-F–NiV-G associations correlated with the fusogenicity of the CT mutants.

We coexpressed NiV-G with WT NiV-F or the aforementioned mutants in permissive 293T cells and determined the relative avidity of NiV-F and NiV-G interactions by immunoprecipitating whole cell lysates with anti-NiV-G antiserum and detecting the amount of co-IP NiV-F by Western blotting with an AU1 epitope tag Ab (Fig. 7A, part a). The relative amounts

of WT and mutant NiV-F were also determined in total cell lysates (Fig. 7A, part b). To normalize for the various expression levels of WT or mutant NiV-F in any single experiment, we calculated the ratio of the level of co-IP NiV-F to the corresponding amount of NiV-F in the total cell lysate. For example, if the amount of co-IP NiV-F was densitometrically quantified at 160 U and the corresponding amount of NiV-F in the cell lysate was 100 U, the F-G co-IP ratio would be 1.6. This ratiometric value was arbitrarily set to 1.0 to indicate the relative avidity of the WT NiV-F–NiV-G interactions (Fig. 7C). On this scale, a value of greater or less than 1.0 would indicate a corresponding increased or decreased avidity in F-G interaction relative to the WT proteins, respectively. Also, we note that the AU1 tag did not affect NiV-F's interaction with G, as the same experiment performed with tagged and untagged NiV-F revealed no difference in the amount of F that can be co-IP with G (Fig. 7B).

When we plotted the relative avidity of NiV-G interactions with WT NiV-F or the indicated CT mutants (Fig. 7C) against their fusogenicities (fusion/CSE ratio) as determined in Table 1, we obtained a significant negative correlation ($r^2 = 0.82$, $P = 0.007$) between the avidity of F-G interaction and the fusogenicity of the NiV-F protein (Fig. 7D). Thus, for example, the NiV-F mutant (K1A) with the lowest relative avidity of F-G interaction (0.4) was also the most fusogenic NiV-F CT mutant examined (fusion/CSE ratio of 5.5), and mutants (K2A and R3A) with the highest relative avidities of F-G interaction (2.1 and 2.6) were the least fusogenic (fusion/CSE ratios of 0.2 and 0.3). These results suggest that the effects of the CT mutants on modulating fusogenicity were linked to the increasing or decreasing avidity of F-G interactions and provide further support for the model (3, 63, 75) where dissociation of the attachment protein from the fusion protein is a rate-limiting step required for fusion peptide exposure and subsequent membrane fusion.

DISCUSSION

Our results implicate the cytoplasmic domain of the NiV fusion protein in modulating fusion through its membrane-proximal polybasic KKR motif in an inside-out signaling manner. Our data also shed some light on the mechanisms by which the KKR motif modulates fusion; specific residues within the KKR motif can modulate the conformation of NiV-F's ectodomain and thus have an effect on fusion kinetics by regulating the rate of 6HB formation and the avidity of the F-G interactions.

The CTs of other paramyxovirus fusion proteins are known to be required for various protein functions, including proper surface expression, membrane fusion, fusion pore enlargement, transition from hemifusion to complete fusion, and/or budding (7, 19, 59, 65, 68), although removal of the CT has resulted in quite distinct phenotypes in different paramyxoviruses, ranging from no effect (12) to fusion pore formation (65) to fusion pore enlargement (19) to syncytium formation (59, 65). In this report, we show that relatively large deletions in the NiV-F CT did not significantly compromise conformational integrity or CSE but can either reduce or enhance fusion (Fig. 1). In addition, while point mutations in the membrane-proximal region had no significant effect on conformational integrity, processing, or CSE, they variably affected fusogenicity (Fig. 2). Indeed, we identified a membrane-proximal polybasic KKR patch in the CT of NiV-F as having the ability to up- or downmodulate fusogenicity. Polybasic residues can also be found near the membrane-spanning region in the CTs of most other paramyxoviruses, but to our knowledge, their function in modulating fusion has not been reported.

Our data show that specific CT mutants with changes in the KKR motif mediate their hyper- or hypofusogenic phenotypes through common mechanisms that have been defined for other class I fusion proteins. For example, the hyperfusogenic V3 loop and CT mutants of the HIV-1 envelope glycoprotein also show faster fusion kinetics and display increased resistance to heptad repeat peptide inhibition (1, 52). In the case of NiV, our results suggest that the hyper- and hypofusogenicity phenotypes of the K1A and K2A mutants are governed by the rate of 6HB formation (Fig. 6A) during fusion pore formation, resulting in increased or decreased fusion kinetics, respectively (Fig. 6B). However, since we did not detect any apparent differences between the R3A mutant and WT NiV-F during 6HB formation and its hypofusogenic phenotype was only manifested in slower fusion kinetics at later time points (Fig. 6B), we speculate that a step post 6HB formation, perhaps fusion pore enlargement, may be affected by the hypofusogenic mutation R3A. The CT of at least one other paramyxovirus, SV5, has been implicated in fusion pore enlargement (19). Our lipid raft results also highlight the mechanistic differences observed between the hypofusogenic K2A and R3A mutants observed in Fig. 4 and 6. The K2A, but not the R3A, mutant displayed differences in lipid raft association compared to the WT NiV-F protein. While many hyper- or hypofusogenic phenotypes in class I viral fusion proteins have been identified, it is uncommon to find a contiguous series of residues within a small patch that have such contrasting contributory roles in fusogenicity.

It remains to be determined how these three basic residues in NiV-F CT actually modulate the kinetics of fusion. Do the KKR mutants stabilize or destabilize the metastable prefusogenic conformation of NiV-F, and/or do they affect subsequent steps in the fusion process? It is also possible that the KKR basic motif may interact with cellular proteins that directly or indirectly modulate the actin cortical cytoskeleton, which is intimately involved in membrane dynamics and curvature during fusion and syncytium formation (37, 49, 51). Dutch and colleagues have previously reported that various transdominant Rho-GTPases can up- or down-regulate HeV fusion (57). Since the ERM (ezrin-radixin-monesin) family of proteins is known to connect the CTs of various membrane proteins to the actin cortical cytoskeleton and the ERM proteins themselves are known to be activated and inactivated by distinct Rho GTPases (21, 29), we speculate that the ERM proteins may connect the CT of NiV-F to the actin cortical cytoskeleton and that modulation of the CT's attachment to the cortical cytoskeleton by the Rho GTPases, or by our various KKR mutants, is what accounts for the hyper- or hypofusogenic phenotypes seen. Intriguingly, ERM proteins preferentially bind CTs of membrane proteins that have isoelectric points higher than 9.0 and that have basic amino acid clusters (29, 74). They also prefer to bind CTs that contain phosphorylated serines and tyrosine motifs (17, 58). NiV-F's CT has an isoelectric point of

9.88, contains a C-terminal tyrosine-rich motif, and contains two basic clusters, i.e., the membrane-proximal KKR cluster that we know affects fusion and an RRVR cluster between regions T3 and T4. In addition, preliminary mass spectrometry analysis indicated that the two C-terminal serines in NiV-F are phosphorylated (unpublished observations). Therefore, it seems plausible that cellular factors such as ERM proteins may connect the CT of NiV-F or HeV-F to the actin cortical cytoskeleton of cells, and the strength and stability of this connection may modulate fusogenicity.

Our data also suggest that the KKR motif modulates fusogenicity via an inside-out signaling mechanism. Differential MAb recognition of the ectodomain correlating with differential neutralization (Fig. 4), faster or slower rates of fusion kinetics affected by the rate of 6HB formation (Fig. 6), and differential effects on the avidity of F-G interactions (Fig. 7) all argue that mutations of these cytoplasmic residues can affect the conformation and subsequent fusogenic function of the ectodomain. Interestingly, data from differential MAb binding, rate of 6HB formation, and fusion kinetics experiments also reveal that distinct mechanisms underlie the similar hypofusogenic phenotypes of the K2A and R3A mutants. For example, while MAbs 92 and 66 clearly bound differentially to the R3A mutant, no difference in K2A binding was observed (Fig. 4B). On the other hand, while K2A was significantly more sensitive to inhibition by HR2-Fc compared to WT NiV-F, R3A was similar in sensitivity to WT NiV-F (Fig. 6A). This equivalent sensitivity to HR2-Fc inhibition is consistent with our real-time fusion kinetics data showing that for the first 40 min, R3A fused at the same rate and to the same extent as WT NiV-F, while K2A fused much more slowly from the very beginning (Fig. 6B). However, after 40 min, R3A began to exhibit slower fusion kinetics and eventually fused to a much lesser extent than WT NiV-F at 100 min. As mentioned above, it is likely that the defect in fusion in the R3A mutant is manifested at a stage post 6HB formation, such as fusion pore enlargement.

We previously suggested that a critical parameter that governs NiV envelope-mediated fusion is the avidity of F and G association, which we quantified by a rigorous coimmunoprecipitation assay (3). Our published data showed a strong and significant negative correlation between the degree of hyperfusogenicity exhibited by a variety of ectodomain N-glycan mutants and the avidity of F and G association. We had therefore favored the attachment protein displacement model of paramyxovirus fusion where the dissociation of G from F after receptor engagement better allows for the conformational changes in F that lead to fusion peptide exposure and membrane fusion. We now provide data to further expand and support this model with both hyper- and hypofusogenic mutants (Fig. 7D). Indeed, as shown in Fig. 7E, when we added our present datum points to the datum points from our hyperfusogenic N-glycan mutants (3), the Pearson correlation became even stronger ($r^2 = 0.91$) and more significant ($P < 0.0001$). These data suggest that F and G dissociation can be a common pathway for the triggering of F regardless of the determinants of fusion in F involved. However, since we performed these studies with receptor-containing 293T cells, we are not able to distinguish whether the differences in F-G association between WT and mutant fusion proteins we have observed occur pre or post receptor binding. True avidity measurements would have to be done with truly receptor-negative cells. In addition, it remains to be determined whether the KKR motif affects the interaction of NiV-F with NiV-G directly and/or via modification of the NiV-F ectodomain's overall conformation. At least for one other paramyxovirus F protein (NDV), the ectodomain HR2 region has been implicated in binding to the attachment protein HN (24); therefore, the effects of NiV-F CT mutants on the avidities of NiV-F–NiV-G interactions observed here may be due to inside-out signaling.

We also note that NiV-F processing is usually increased when G is cotransfected (compare Fig. 7A with Fig. 1B and 2B). Since both F and G are encoded by codon-optimized genes, a potential explanation is that expression of G competes for transcriptional or translational resources, resulting in less overexpression of F; overexpression of F in the absence of G can overwhelm the proteolytic machinery required for F cleavage. However, it would be interesting to determine whether the presence of G, and its association with F, can intrinsically affect F processing, either by modulating its endosomal recycling behavior or changing the conformation of F to make it more accessible to cathepsin L cleavage.

Finally, it remains to be determined how the NiV-F CT actually stabilizes or destabilizes F-G interactions and whether the fusion-modulatory role played by the polybasic motif in the CT of NiV-F is unique for NiV (or the henipaviruses). The studies presented in this report point to the many determinants of fusion in NiV-F and underscore the complexities that regulate the "proper" amount of fusion mediated by NiV-F, which has both fusion-promoting and fusion-inhibiting determinants. Further studies of these determinants will enhance our understanding of the pathobiology of this deadly emerging virus and may reveal more targets for therapeutic intervention.

ACKNOWLEDGMENTS

This study was supported by NIH grants AI059051, AI060694, and AI069317 to B.L. Additional support was provided by a Charles E. Culpepper Medical Scholarship from the Rockefeller Brothers Fund and a Burroughs Wellcome Fund Career Development Award. We acknowledge support from the UCLA AIDS Institute and the CFAR flow cytometry core supported by NIH grants CA16042 and AI28697.

REFERENCES

1. **Abrahamyan, L. G., S. R. Mkrtchyan, J. Binley, M. Lu, G. B. Melikyan, and F. S. Cohen.** 2005. The cytoplasmic tail slows the folding of human immunodeficiency virus type 1 Env from a late prebundle configuration into the six-helix bundle. J. Virol. **79:**106–115.
2. **Aguilar, H. C., W. F. Anderson, and P. M. Cannon.** 2003. Cytoplasmic tail of Moloney murine leukemia virus envelope protein influences the conformation of the extracellular domain: implications for mechanism of action of the R Peptide. J. Virol. **77:**1281–1291.
3. **Aguilar, H. C., K. A. Matreyek, C. M. Filone, S. T. Hashimi, E. L. Levroney, O. A. Negrete, A. Bertolotti-Ciarlet, D. Y. Choi, I. McHardy, J. A. Fulcher, S. V. Su, M. C. Wolf, L. Kohatsu, L. G. Baum, and B. Lee.** 2006. N-glycans on Nipah virus fusion protein protect against neutralization but reduce membrane fusion and viral entry. J. Virol. **80:**4878–4889.
4. **Aguilar, H. C., O. A. Negrete, K. A. Matreyek, D. Y. Choi, and B. Lee.** 2006. Novel rabbit monoclonal antibodies against the henipavirus envelope glycoproteins reveal conformational epitopes related to fusogenicity and receptor binding, abstr. P19-4. *In* American Society for Virology, 25th Annual Meeting. American Society for Virology, Madison, WI.
5. **Anonymous.** 28 April 2004, posting date. NIPAH virus breaks out in Bangladesh: mortality rates of 60% to 74%. Human to-human transmission may be implicated. Wildlife Trust. www.ewire.com/display.cfm/WirelowemID/2117. [Online.]
6. **Anonymous.** 2004. Nipah virus outbreak(s) in Bangladesh, January-April 2004. Wkly. Epidemiol. Rec. **79:**168–171.
7. **Bagai, S., and R. A. Lamb.** 1996. Truncation of the COOH-terminal region

of the paramyxovirus SV5 fusion protein leads to hemifusion but not complete fusion. J. Cell Biol. **135:**73–84.
8. **Baker, K. A., R. E. Dutch, R. A. Lamb, and T. S. Jardetzky.** 1999. Structural basis for paramyxovirus-mediated membrane fusion. Mol. Cell **3:**309–319.
9. **Bonaparte, M. I., A. S. Dimitrov, K. N. Bossart, G. Crameri, B. A. Mungall, K. A. Bishop, V. Choudhry, D. S. Dimitrov, L. F. Wang, B. T. Eaton, and C. C. Broder.** 2005. Ephrin-B2 ligand is a functional receptor for Hendra virus and Nipah virus. Proc. Natl. Acad. Sci. USA **102:**10652–10657.
10. **Bossart, K. N., L. F. Wang, B. T. Eaton, and C. C. Broder.** 2001. Functional expression and membrane fusion tropism of the envelope glycoproteins of Hendra virus. Virology **290:**121–135.
11. Reference deleted.
12. **Branigan, P. J., N. D. Day, C. Liu, L. L. Gutshall, J. A. Melero, R. T. Sarisky, and A. M. Del Vecchio.** 2006. The cytoplasmic domain of the F protein of human respiratory syncytial virus is not required for cell fusion. J. Gen. Virol. **87:**395–398.
13. **Brody, B. A., S. S. Rhee, and E. Hunter.** 1994. Postassembly cleavage of a retroviral glycoprotein cytoplasmic domain removes a necessary incorporation signal and activates fusion activity. J. Virol. **68:**4620–4627.
14. **Carr, C. M., and P. S. Kim.** 1993. A spring-loaded mechanism for the conformational change of influenza hemagglutinin. Cell **73:**823–832.
15. **Carter, J. R., C. T. Pager, S. D. Fowler, and R. E. Dutch.** 2005. Role of N-linked glycosylation of the Hendra virus fusion protein. J. Virol. **79:**7922–7925.
16. **Chakrabarti, L., M. Emerman, P. Tiollais, and P. Sonigo.** 1989. The cytoplasmic domain of simian immunodeficiency virus transmembrane protein modulates infectivity. J. Virol. **63:**4395–4403.
17. **Dickson, T. C., C. D. Mintz, D. L. Benson, and S. R. Salton.** 2002. Functional binding interaction identified between the axonal CAM L1 and members of the ERM family. J. Cell Biol. **157:**1105–1112.
18. **Diederich, S., M. Moll, H. D. Klenk, and A. Maisner.** 2005. The Nipah virus fusion protein is cleaved within the endosomal compartment. J. Biol. Chem. **280:**29899–29903.
19. **Dutch, R. E., and R. A. Lamb.** 2001. Deletion of the cytoplasmic tail of the fusion protein of the paramyxovirus simian virus 5 affects fusion pore enlargement. J. Virol. **75:**5363–5369.
20. **Fass, D., S. C. Harrison, and P. S. Kim.** 1996. Retrovirus envelope domain at 1.7 Angstrom resolution. Nat. Struct. Biol. **3:**465–469.
21. **Faure, S., L. I. Salazar-Fontana, M. Semichon, V. L. Tybulewicz, G. Bismuth, A. Trautmann, R. N. Germain, and J. Delon.** 2004. ERM proteins regulate cytoskeleton relaxation promoting T cell-APC conjugation. Nat. Immunol. **5:**272–279.
22. **Fleming, E. H., A. A. Kolokoltsov, R. A. Davey, J. E. Nichols, and N. J. Roberts, Jr.** 2006. Respiratory syncytial virus F envelope protein associates with lipid rafts without a requirement for other virus proteins. J. Virol. **80:**12160–12170.
23. **Gandhavadi, M., D. Allende, A. Vidal, S. A. Simon, and T. J. McIntosh.** 2002. Structure, composition, and peptide binding properties of detergent soluble bilayers and detergent resistant rafts. Biophys. J. **82:**1469–1482.
24. **Gravel, K. A., and T. G. Morrison.** 2003. Interacting domains of the HN and F proteins of Newcastle disease virus. J. Virol. **77:**11040–11049.
25. **Green, N., T. M. Shinnick, O. Witte, A. Ponticelli, J. G. Sutcliffe, and R. A. Lerner.** 1981. Sequence-specific antibodies show that maturation of Moloney leukemia virus envelope polyprotein involves removal of a COOH-terminal peptide. Proc. Natl. Acad. Sci. USA **78:**6023–6027.
26. **Hawkes, D. J., and J. Mak.** 2006. Lipid membrane; a novel target for viral and bacterial pathogens. Curr. Drug Targets **7:**1615–1621.
27. **Horvath, C. M., R. G. Paterson, M. A. Shaughnessy, R. Wood, and R. A. Lamb.** 1992. Biological activity of paramyxovirus fusion proteins: factors influencing formation of syncytia. J. Virol. **66:**4564–4569.
28. **Ito, M., M. Nishio, H. Komada, Y. Ito, and M. Tsurudome.** 2000. An amino acid in the heptad repeat 1 domain is important for the haemagglutinin-neuraminidase-independent fusing activity of simian virus 5 fusion protein. J. Gen. Virol. **81:**719–727.
29. **Ivetic, A., and A. J. Ridley.** 2004. Ezrin/radixin/moesin proteins and Rho GTPase signalling in leucocytes. Immunology **112:**165–176.
30. **Jacobson, K., O. G. Mouritsen, and R. G. Anderson.** 2007. Lipid rafts: at a crossroad between cell biology and physics. Nat. Cell Biol. **9:**7–14.
31. **Kodama, T., D. P. Burns, H. W. Kestler III, M. D. Daniel, and R. C. Desrosiers.** 1990. Molecular changes associated with replication of simian immunodeficiency virus in human cells. J. Med. Primatol. **19:**431–437.
32. **Lam, S. K.** 2003. Nipah virus—a potential agent of bioterrorism? Antiviral Res. **57:**113–119.
33. **Levroney, E. L., H. C. Aguilar, J. A. Fulcher, L. Kohatsu, K. E. Pace, M. Pang, K. B. Gurney, L. G. Baum, and B. Lee.** 2005. Novel innate immune functions for galectin-1: galectin-1 inhibits cell fusion by Nipah virus envelope glycoproteins and augments dendritic cell secretion of proinflammatory cytokines. J. Immunol. **175:**413–420.
34. **Lineberger, J. E., R. Danzeisen, D. J. Hazuda, A. J. Simon, and M. D. Miller.** 2002. Altering expression levels of human immunodeficiency virus type 1 gp120-gp41 affects efficiency but not kinetics of cell-cell fusion. J. Virol. **76:**3522–3533.
35. **Lou, Z., Y. Xu, K. Xiang, N. Su, L. Qin, X. Li, G. F. Gao, M. Bartlam, and Z. Rao.** 2006. Crystal structures of Nipah and Hendra virus fusion core proteins. FEBS J. **273:**4538–4547.
36. **Mebatsion, T., S. Finke, F. Weiland, and K. K. Conzelmann.** 1997. A CXCR4/CD4 pseudotype rhabdovirus that selectively infects HIV-1 envelope protein-expressing cells. Cell **90:**841–847.
37. **Melikyan, G. B., S. A. Brener, D. C. Ok, and F. S. Cohen.** 1997. Inner but not outer membrane leaflets control the transition from glycosylphosphatidylinositol-anchored influenza hemagglutinin-induced hemifusion to full fusion. J. Cell Biol. **136:**995–1005.
38. **Melikyan, G. B., R. M. Markosyan, H. Hemmati, M. K. Delmedico, D. M. Lambert, and F. S. Cohen.** 2000. Evidence that the transition of HIV-1 gp41 into a six-helix bundle, not the bundle configuration, induces membrane fusion. J. Cell Biol. **151:**413–423.
39. **Meulendyke, K. A., M. A. Wurth, R. O. McCann, and R. E. Dutch.** 2005. Endocytosis plays a critical role in proteolytic processing of the Hendra virus fusion protein. J. Virol. **79:**12643–12649.
40. **Moll, M., A. Kaufmann, and A. Maisner.** 2004. Influence of N-glycans on processing and biological activity of the Nipah virus fusion protein. J. Virol. **78:**7274–7278.
41. **Mulligan, M. J., G. V. Yamshchikov, G. D. Ritter, Jr., F. Gao, M. J. Jin, C. D. Nail, C. P. Spies, B. H. Hahn, and R. W. Compans.** 1992. Cytoplasmic domain truncation enhances fusion activity by the exterior glycoprotein complex of human immunodeficiency virus type 2 in selected cell types. J. Virol. **66:**3971–3975.
42. **Murakami, T., S. Ablan, E. O. Freed, and Y. Tanaka.** 2004. Regulation of human immunodeficiency virus type 1 Env-mediated membrane fusion by viral protease activity. J. Virol. **78:**1026–1031.
43. **Nayak, D. P., and S. Barman.** 2002. Role of lipid rafts in virus assembly and budding. Adv. Virus Res. **58:**1–28.
44. **Negrete, O. A., E. L. Levroney, H. C. Aguilar, A. Bertolotti-Ciarlet, R. Nazarian, S. Tajyar, and B. Lee.** 2005. EphrinB2 is the entry receptor for Nipah virus, an emergent deadly paramyxovirus. Nature **436:**401–405.
45. **Negrete, O. A., M. C. Wolf, H. C. Aguilar, S. Enterlein, W. Wang, E. Muhlberger, S. V. Su, A. Bertolotti-Ciarlet, R. Flick, and B. Lee.** 2006. Two key residues in ephrinB3 are critical for its use as an alternative receptor for Nipah virus. PLoS Pathogens **2:**e7.
46. **Olson, J. G., C. Rupprecht, P. E. Rollin, U. S. An, M. Niezgoda, T. Clemins, J. Walston, and T. G. Ksiazek.** 2002. Antibodies to Nipah-like virus in bats (Pteropus lylei), Cambodia. Emerg. Infect. Dis. **8:**987–988.
47. **Ono, A., and E. O. Freed.** 2001. Plasma membrane rafts play a critical role in HIV-1 assembly and release. Proc. Natl. Acad. Sci. USA **98:**13925–13930.
48. **Paterson, R. G., S. W. Hiebert, and R. A. Lamb.** 1985. Expression at the cell surface of biologically active fusion and hemagglutinin/neuraminidase proteins of the paramyxovirus simian virus 5 from cloned cDNA. Proc. Natl. Acad. Sci. USA **82:**7520–7524.
49. **Pontow, S. E., N. V. Heyden, S. Wei, and L. Ratner.** 2004. Actin cytoskeletal reorganizations and coreceptor-mediated activation of Rac during human immunodeficiency virus-induced cell fusion. J. Virol. **78:**7138–7147.
50. **Ragheb, J. A., and W. F. Anderson.** 1994. pH-independent murine leukemia virus ecotropic envelope-mediated cell fusion: implications for the role of the R peptide and p12E TM in viral entry. J. Virol. **68:**3220–3231.
51. **Razinkov, V. I., G. B. Melikyan, R. M. Epand, R. F. Epand, and F. S. Cohen.** 1998. Effects of spontaneous bilayer curvature on influenza virus-mediated fusion pores. J. Gen. Physiol. **112:**409–422.
52. **Reeves, J. D., S. A. Gallo, N. Ahmad, J. L. Miamidian, P. E. Harvey, M. Sharron, S. Pohlmann, J. N. Sfakianos, C. A. Derdeyn, R. Blumenthal, E. Hunter, and R. W. Doms.** 2002. Sensitivity of HIV-1 to entry inhibitors correlates with envelope/coreceptor affinity, receptor density, and fusion kinetics. Proc. Natl. Acad. Sci. USA **99:**16249–16254.
53. **Reeves, J. D., J. L. Miamidian, M. J. Biscone, F. H. Lee, N. Ahmad, T. C. Pierson, and R. W. Doms.** 2004. Impact of mutations in the coreceptor binding site on human immunodeficiency virus type 1 fusion, infection, and entry inhibitor sensitivity. J. Virol. **78:**5476–5485.
54. **Rein, A., J. Mirro, J. G. Haynes, S. M. Ernst, and K. Nagashima.** 1994. Function of the cytoplasmic domain of a retroviral transmembrane protein: p15E-p2E cleavage activates the membrane fusion capability of the murine leukemia virus Env protein. J. Virol. **68:**1773–1781.
55. **Russell, C. J., T. S. Jardetzky, and R. A. Lamb.** 2001. Membrane fusion machines of paramyxoviruses: capture of intermediates of fusion. EMBO J. **20:**4024–4034.
56. **Schnell, M. J., J. E. Johnson, L. Buonocore, and J. K. Rose.** 1997. Construction of a novel virus that targets HIV-1-infected cells and controls HIV-1 infection. Cell **90:**849–857.
57. **Schowalter, R. M., M. A. Wurth, H. C. Aguilar, B. Lee, C. L. Moncman, R. O. McCann, and R. E. Dutch.** 2006. Rho GTPase activity modulates paramyxovirus fusion protein-mediated cell-cell fusion. Virology **350:**323–334.
58. **Serrador, J. M., M. Vicente-Manzanares, J. Calvo, O. Barreiro, M. C. Montoya, R. Schwartz-Albiez, H. Furthmayr, F. Lozano, and F. Sanchez-Madrid.** 2002. A novel serine-rich motif in the intercellular adhesion molecule 3 is critical for its ezrin/radixin/moesin-directed subcellular targeting. J. Biol. Chem. **277:**10400–10409.

59. **Seth, S., A. Vincent, and R. W. Compans.** 2003. Mutations in the cytoplasmic domain of a paramyxovirus fusion glycoprotein rescue syncytium formation and eliminate the hemagglutinin-neuraminidase protein requirement for membrane fusion. J. Virol. **77:**167–178.
60. **Shimizu, H., F. Hasebe, H. Tsuchie, S. Morikawa, H. Ushijima, and T. Kitamura.** 1992. Analysis of a human immunodeficiency virus type 1 isolate carrying a truncated transmembrane glycoprotein. Virology **189:**534–546.
61. **Spies, C. P., G. D. Ritter, Jr., M. J. Mulligan, and R. W. Compans.** 1994. Truncation of the cytoplasmic domain of the simian immunodeficiency virus envelope glycoprotein alters the conformation of the external domain. J. Virol. **68:**585–591.
62. **Takeda, M., G. P. Leser, C. J. Russell, and R. A. Lamb.** 2003. Influenza virus hemagglutinin concentrates in lipid raft microdomains for efficient viral fusion. Proc. Natl. Acad. Sci. USA **100:**14610–14617.
63. **Takimoto, T., G. L. Taylor, H. C. Connaris, S. J. Crennell, and A. Portner.** 2002. Role of the hemagglutinin-neuraminidase protein in the mechanism of paramyxovirus-cell membrane fusion. J. Virol. **76:**13028–13033.
64. **Tan, C. T., and K. T. Wong.** 2003. Nipah encephalitis outbreak in Malaysia. Ann. Acad. Med. Singapore **32:**112–117.
65. **Tong, S., M. Li, A. Vincent, R. W. Compans, E. Fritsch, R. Beier, C. Klenk, M. Ohuchi, and H. D. Klenk.** 2002. Regulation of fusion activity by the cytoplasmic domain of a paramyxovirus F protein. Virology **301:**322–333.
66. **Wang, L. F., M. Yu, E. Hansson, L. I. Pritchard, B. Shiell, W. P. Michalski, and B. T. Eaton.** 2000. The exceptionally large genome of Hendra virus: support for creation of a new genus within the family *Paramyxoviridae*. J. Virol. **74:**9972–9979.
67. **Waning, D. L., C. J. Russell, T. S. Jardetzky, and R. A. Lamb.** 2004. Activation of a paramyxovirus fusion protein is modulated by inside-out signaling from the cytoplasmic tail. Proc. Natl. Acad. Sci. USA **101:**9217–9222.
68. **Waning, D. L., A. P. Schmitt, G. P. Leser, and R. A. Lamb.** 2002. Roles for the cytoplasmic tails of the fusion and hemagglutinin-neuraminidase proteins in budding of the paramyxovirus simian virus 5. J. Virol. **76:**9284–9297.
69. **Wessel, D., and U. I. Flugge.** 1984. A method for the quantitative recovery of protein in dilute solution in the presence of detergents and lipids. Anal. Biochem. **138:**141–143.
70. **Wong, K. T., W. J. Shieh, S. Kumar, K. Norain, W. Abdullah, J. Guarner, C. S. Goldsmith, K. B. Chua, S. K. Lam, C. T. Tan, K. J. Goh, H. T. Chong, R. Jusoh, P. E. Rollin, T. G. Ksiazek, and S. R. Zaki.** 2002. Nipah virus infection: pathology and pathogenesis of an emerging paramyxoviral zoonosis. Am. J. Pathol. **161:**2153–2167.
71. **Wyss, S., A. S. Dimitrov, F. Baribaud, T. G. Edwards, R. Blumenthal, and J. A. Hoxie.** 2005. Regulation of human immunodeficiency virus type 1 envelope glycoprotein fusion by a membrane-interactive domain in the gp41 cytoplasmic tail. J. Virol. **79:**12231–12241.
72. **Yin, H. S., R. G. Paterson, X. Wen, R. A. Lamb, and T. S. Jardetzky.** 2005. Structure of the uncleaved ectodomain of the paramyxovirus (hPIV3) fusion protein. Proc. Natl. Acad. Sci. USA **102:**9288–9293.
73. **Yin, H. S., X. Wen, R. G. Paterson, R. A. Lamb, and T. S. Jardetzky.** 2006. Structure of the parainfluenza virus 5 F protein in its metastable, prefusion conformation. Nature **439:**38–44.
74. **Yonemura, S., M. Hirao, Y. Doi, N. Takahashi, T. Kondo, and S. Tsukita.** 1998. Ezrin/radixin/moesin (ERM) proteins bind to a positively charged amino acid cluster in the juxta-membrane cytoplasmic domain of CD44, CD43, and ICAM-2. J. Cell Biol. **140:**885–895.
75. **Zaitsev, V., M. von Itzstein, D. Groves, M. Kiefel, T. Takimoto, A. Portner, and G. Taylor.** 2004. Second sialic acid binding site in Newcastle disease virus hemagglutinin-neuraminidase: implications for fusion. J. Virol. **78:**3733–3741.
76. **Zingler, K., and D. R. Littman.** 1993. Truncation of the cytoplasmic domain of the simian immunodeficiency virus envelope glycoprotein increases Env incorporation into particles and fusogenicity and infectivity. J. Virol. **67:**2824–2831.